Article

Cell Reports

Defects in the *CAPN1* Gene Result in Alterations in Cerebellar Development and Cerebellar Ataxia in Mice and Humans

Graphical Abstract

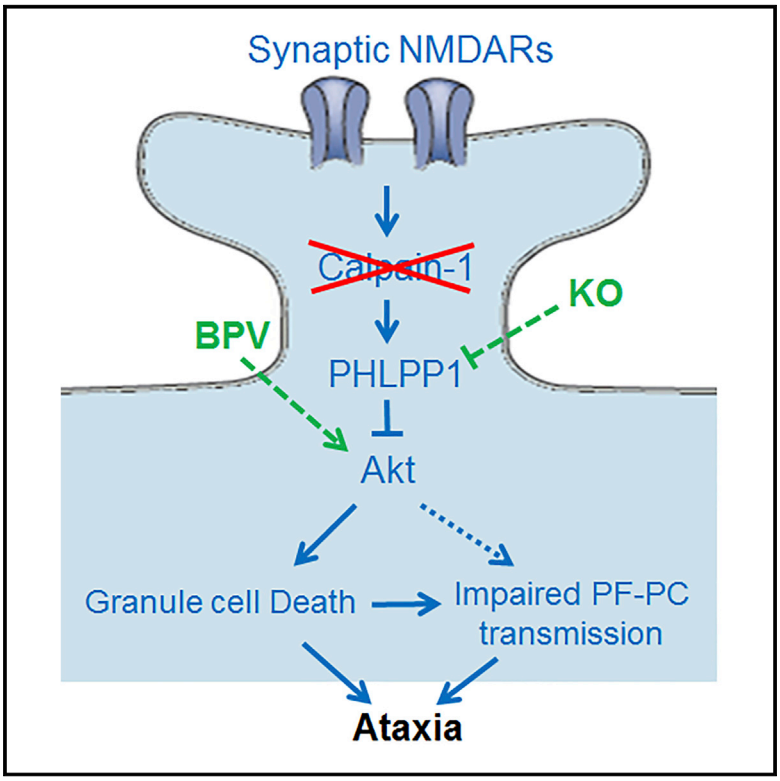

Authors

Yubin Wang, Joshua Hersheson, Dulce Lopez, ..., Xiaoning Bi, Henry Houlden, Michel Baudry

Correspondence

h.houlden@ucl.ac.uk (H.H.), mbaudry@westernu.edu (M.B.)

In Brief

Wang et al. report that deletion and mutations of *CAPN1* results in alterations in cerebellar development and cerebellar ataxia in humans and mice due to enhanced developmental apoptosis of cerebellar granule cells caused by lack of calpain-1-mediated Akt activation and altered adult cerebellar function. Restoring Akt activation reverses apoptosis and ataxia.

Highlights

- Null calpain-1 mutations result in cerebellar ataxia in humans and mice
- Ataxia is due to altered cerebellar development and adult function
- Calpain-1-mediated truncation of PHLPP1 and Akt activation limits postnatal apoptosis
- Pharmacologic or genetic Akt activation reverses developmental alterations and ataxia

Wang et al., 2016, Cell Reports *16*, 79–91
June 28, 2016
http://dx.doi.org/10.1016/j.celrep.2016.05.044

CellPress

Cell Reports
Article

Defects in the *CAPN1* Gene Result in Alterations in Cerebellar Development and Cerebellar Ataxia in Mice and Humans

Yubin Wang,[1] Joshua Hersheson,[3] Dulce Lopez,[1] Monia Hammer,[5,6] Yan Liu,[1] Ka-Hung Lee,[1] Vanessa Pinto,[2] Jeff Seinfeld,[1] Sarah Wiethoff,[3,4] Jiandong Sun,[2] Rim Amouri,[5] Faycal Hentati,[5] Neema Baudry,[1] Jennifer Tran,[1] Andrew B. Singleton,[6] Marie Coutelier,[7,8,9] Alexis Brice,[7,10] Giovanni Stevanin,[7,9,10] Alexandra Durr,[7,10] Xiaoning Bi,[2] Henry Houlden,[3,11,*] and Michel Baudry[1,11,*]

[1]Graduate College of Biomedical Sciences
[2]College of Osteopathic Medicine of the Pacific
Western University of Health Sciences, Pomona, CA 91766, USA
[3]The National Hospital for Neurology and Neurosurgery and UCL Institute of Neurology, Queen Square, London WC1N 3BG, UK
[4]Center for Neurology and Hertie Institute for Clinical Brain Research, Eberhard-Karls-University, 72076 Tübingen, Germany
[5]Department of Molecular Neurobiology and Neuropathology, National Institute of Neurology, La Rabta, Tunis 1007, Tunisia
[6]Laboratory of Neurogenetics, National Institutes of Health, Bethesda 20892, MD, USA
[7]INSERM U 1127, CNRS UMR 7225, Sorbonne Universités, Université Pierre et Marie Curie Paris 06 UMRS 1127, Institut du Cerveau et de la Moelle épinière, 75013 Paris, France
[8]Laboratory of Human Molecular Genetics, de Duve Institute, Université Catholique de Louvain, 1200 Brussels, Belgium
[9]Ecole Pratique des Hautes Etudes (EPHE), Paris Sciences et Lettres (PSL) Research University, 75013 Paris, France
[10]Centre de Référence de Neurogénétique, Hôpital de la Pitié-Salpêtrière, Assistance Publique – Hôpitaux de Paris, 75013 Paris, France
[11]Co-senior author
*Correspondence: h.houlden@ucl.ac.uk (H.H.), mbaudry@westernu.edu (M.B.)
http://dx.doi.org/10.1016/j.celrep.2016.05.044

SUMMARY

A *CAPN1* missense mutation in Parson Russell Terrier dogs is associated with spinocerebellar ataxia. We now report that homozygous or heterozygous *CAPN1*-null mutations in humans result in cerebellar ataxia and limb spasticity in four independent pedigrees. Calpain-1 knockout (KO) mice also exhibit a mild form of ataxia due to abnormal cerebellar development, including enhanced neuronal apoptosis, decreased number of cerebellar granule cells, and altered synaptic transmission. Enhanced apoptosis is due to absence of calpain-1-mediated cleavage of PH domain and leucine-rich repeat protein phosphatase 1 (PHLPP1), which results in inhibition of the Akt pro-survival pathway in developing granule cells. Injection of neonatal mice with the indirect Akt activator, bisperoxovanadium, or crossing calpain-1 KO mice with PHLPP1 KO mice prevented increased postnatal cerebellar granule cell apoptosis and restored granule cell density and motor coordination in adult mice. Thus, mutations in *CAPN1* are an additional cause of ataxia in mammals, including humans.

INTRODUCTION

Calpains are calcium-dependent proteases playing both physiological and pathological roles in the CNS (Liu et al., 2008; Wang et al., 2013; Wang et al., 2014). Two major calpain isoforms are present in CNS, calpain-1 and calpain-2, which differ in their calcium requirements for activation. Calpain activity is higher in cerebellum than in cortex or hippocampus across different mammalian species (Baudry et al., 1986). Immunohistochemistry study revealed that the major calpain isoform expressed in cerebellar neurons is calpain-1 (Hamakubo et al., 1986). Calpain-1 activity in cerebellum during prenatal and early postnatal period is high, as compared to that in adulthood (Simonson et al., 1985), suggesting a potential role for calpain-1 in cerebellar development. Interestingly, a *CAPN1* missense mutation in the Parson Russell Terrier dog breed has been associated with spinocerebellar ataxia (Forman et al., 2013).

Loss of cerebellar granule cells (CGCs) induced by different mechanisms results in ataxia (Hashimoto et al., 1999; Kim et al., 2009; Pennacchio et al., 1998; Shmerling et al., 1998). NMDA receptor (NMDAR) activity is essential for CGC survival during the critical stage of cerebellar development (Balázs et al., 1988; Monti and Contestabile, 2000; Monti et al., 2002; Moran and Patel, 1989), although the underlying mechanism remains elusive. NMDAR-induced activation of the nuclear factor CREB is required (Monti et al., 2002), and CREB is a target of the pro-survival kinase Akt (Du and Montminy, 1998).

Synaptic NMDAR-mediated calpain-1 activation results in the degradation of the PH domain and leucine-rich repeat protein phosphatase 1 (PHLPP1). PHLPP1 dephosphorylates and inhibits Akt and is involved in tumorigenesis (Chen et al., 2011), circadian clock (Masubuchi et al., 2010), learning and memory process (Shimizu et al., 2007; Wang et al., 2014), and autophagy (Arias et al., 2015). Calpain-1-mediated degradation of PHLPP1 activates Akt and promotes neuronal survival (Wang et al., 2013),

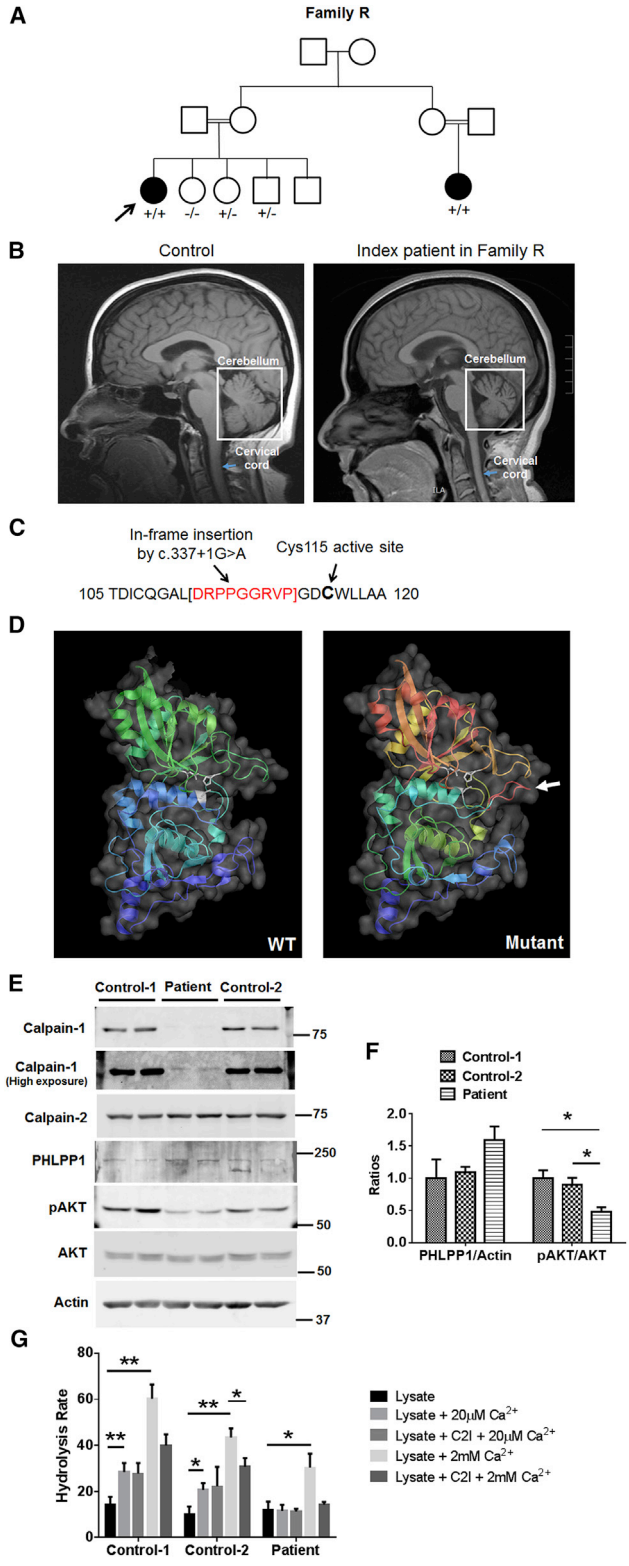

Figure 1. Mutation in *CANP1* Gene in Family R Results in Lack of Calpain-1 Expression and Activity

(A) Pedigree of family R. There are at least two consanguineous loops where the parents of affected individuals are cousins. Square, male; circle, female; black symbols, affected; arrow, proband. +/+, homozygous for the mutation; +/−, heterozygous for the mutation; −/−, homozygous wild-type.

(B) Sagittal T1 MRI from unaffected control (left) and affected proband (right). MRI on the proband shows cerebellar atrophy and cervical spinal cord thinning; repeat MRIs showed the atrophy slowly progressed over time.

(C) Homozygous splice site mutation causes an in-frame insert (arrow) in close proximity to the Cys115 active site (arrow).

(D) Three-dimensional structure of WT CAPN1 protein and predicted mutant protein showing loss of active site (arrow).

(E) Western blot for calpain-1, calpain-2, PHLPP1, phospho-Akt S473 (pAkt), total Akt and actin in fibroblasts from patient RK38, and two control human subjects.

(F) Quantitative analysis of the ratios of PHLPP1 to actin, and pAkt to Akt in each cell line. Results represent means ± SEM of four experiments. The replicates are different cell batches from the same patient or controls. *$p < 0.05$. One-way ANOVA followed by Bonferroni test.

(G) Calpain-1 and -2 activities were determined in lysates of cultured fibroblasts from control or affected subjects as indicated in Experimental Procedures. Results represent means ± SEM of four experiments. *$p < 0.05$, **$p < 0.01$. One-way ANOVA followed by Bonferroni test.

and we postulated that calpain-1-mediated regulation of PHLPP1 and Akt could be involved in NMDAR-dependent CGC survival during postnatal development.

Here, we report that calpain-1 KO mice exhibit abnormal cerebellar development, including enhanced apoptosis of CGCs during the early postnatal period, reduced granule cell density and impaired synaptic transmission from parallel fiber to Purkinje cells, resulting in an ataxia phenotype. All these defects are due to deficits in the calpain-1/PHLPP1/Akt pro-survival pathway in developing granule cells, since treatment with an Akt activator during the postnatal period or crossing calpain-1 KO mice with PHLPP1 KO mice restores most of the observed alterations in cerebellar structure and function in calpain-1 KO mice. We also report four human families carrying homozygous or heterozygous compound *CAPN1* mutations segregating with cerebellar ataxia. These findings indicate that *CAPN1* is an additional gene for cerebellar ataxia.

RESULTS

Four Human Pedigrees of Spastic Ataxia with Calpain-1-Null Mutations

Blood samples and DNA were extracted from affected and unaffected family members with informed consent (institutional review board/ethics 06/N076). The index patient in family R (Figure 1A) is currently 43 years old and of Bangladeshi origin, living in the UK. The proband first presented with gait ataxia, spasticity, and dysphagia in her late teens with slow symptom progression over the subsequent years. She is now a wheelchair user with severe ataxia and cerebellar and bulbar dysarthria, and she falls and exhibits spasticity. There is mild cognitive decline on clinical and standard psychometric IQ testing. MRI investigations showed mild cerebellar atrophy (Figure 1B). Electromyography and nerve conduction studies were normal. Standard screening prior to mapping and exome sequencing included negative testing for SCA1, 2, 3, 6, 7, 8, 11, 12, 14, 17, FRDA, AOA1, AOA2, ATM, and common mitochondrial mutations.

Homozygosity mapping across the genome was carried out using DNA SNP arrays (Illumina) and identified shared regions

of homozygosity with a number of variants between the two affected individuals in family R. Exome sequencing was carried out to a depth of 50× coverage, and variants were filtered according to a number of parameters, including the homozygous regions in both affected individuals. They shared a homozygous splice mutation in *CAPN1* (exon3:c.337+1G > A), predicted to interfere with normal RNA splicing.

cDNA was synthesized from RNA extracted from a peripheral blood sample from the index patient in family R. Primers designed to amplify across the splice site were used to show that the variant results in retention of part of the intron producing an in-frame insertion of nine amino acids (Figure 1C). Homology modeling of the mutant protein was performed using SwissModel and was based on the established crystal structure for calpain-1. The nine-amino-acid insertion was located close to the active site and visualization of the mutant protein structure shows that the additional peptide loop would sterically block the active site cleft (Figure 1D). Besides the two patients in family R mentioned above, we found *CAPN1* mutations in three additional pedigrees. One Italian patient (SAL-584-005) harbored a NM_001198868:c.183dupC homozygous frameshift variant, two Tunisian siblings (Tun66273 and Tun66275) presented with a NM_001198868:c.1534C > T homozygous missense mutation, and one proband from French and Spanish ascent (SAL-399-073) carried a NM_001198868:c.C463T nonsense variant (Q155X) in *trans* with a NM_001198868:c.C1142T missense change. Reported missense mutations are respectively responsible for arginine 512 to cysteine (R512C) and alanine 381 to valine (A381V) substitutions in calpain-1, which may both disrupt the protein function. All these families have similar clinical presentations with progressive spastic ataxia, associated with mild axonal peripheral involvement and slow ocular saccades in one family. We further describe them in the Supplemental Information (Figures S1–S3).

Fibroblasts were isolated from the skin biopsy of the index patient in family R and two control humans. Levels of calpain-1, calpain-2, PHLPP1, and Akt in fibroblast lysates were examined with western blot (Figures 1E and 1F). Surprisingly, calpain-1 expression was completely absent in patient fibroblasts. There was a faint band slightly higher than the normal calpain-1 band found in control fibroblasts (Figure 1E, calpain-1 high exposure), which is possibly the mutated calpain-1 with the nine-amino-acid insert. These results suggest that the mutated calpain-1 protein is unstable and rapidly degraded after synthesis. Calpain-2 level was normal in the patient cell line, as compared to two control cell lines. The level of PHLPP1, a specific substrate of calpain-1 (Wang et al., 2013), was slightly but not significantly increased, and the level of phospho-Akt Ser473 (pAkt), which can be dephosphorylated by PHLPP1, was significantly decreased in patient fibroblasts, as compared to control fibroblasts. Calpain activity in fibroblast lysates was measured with a fluorescent substrate, Suc-Leu-Tyr-AMC (Figure 1G), in the presence of 20 μM or 2 mM free Ca^{2+}, respectively. While calpain-1 activity was present in control cell lines, it was absent in the patient cell line. Calpain-2 activity was present in all cell lines. A calpain-2 selective inhibitor (C2I) Z-Leu-Abu-CONH-CH_2-C_6H_3 (3, 5-$(OMe)_2$) (Wang et al., 2014) was used to confirm the absence of calpain-1 in the patient cell line.

Calpain-1 KO Mice Exhibit Ataxia

To test whether lack of calpain-1 could result in ataxia in mice, motor performance of calpain-1 KO and wild-type (WT) mice was evaluated by rotarod and gait tests. Calpain-1 KO mice exhibited a slight but not significant reduced latency to fall from a rotating rod at 3 months of age (Figure 2A). At 7 months of age, KO mice exhibited a significantly shorter latency to fall from trial days 3 to 7, as compared to age-matched WT mice (Figure 2B). Calpain-1 KO mice also had shorter strides and stances and longer sways at all tested ages (3, 5, 6, and 7 months), as compared to WT mice (Figures 2C–2E).

Calpain-1 KO Mice Exhibit Enhanced Apoptosis of CGCs during Postnatal Development and Reduced CGC Density in Adulthood

Blockade of NMDAR during postnatal development exacerbates the normal apoptotic elimination of CGCs in rats (Monti and Contestabile, 2000). We first repeated this result with multiple intraperitoneal (i.p.) injections of the NMDAR antagonist MK801 (0.5 mg/kg) before postnatal days (PNDs) 3, 7, or 10 in WT mice. After three injections at 24, 16, and 8 hr before PND 3, 7, or 10, enhanced apoptosis was evident in the external and internal granular layer of cerebellum in MK801-injected mice at PND7 (Figures 3A and 3C) and 10 (Figures 3B and 3C) but not PND3 (Figure 3C), a result consistent with the findings in rats. To determine whether calpain-1 was involved in NMDAR-mediated survival in developing cerebellum, we analyzed neuronal apoptosis in cerebellum of calpain-1 KO mice at PND3, 7, and 10. Enhanced apoptosis was found in the cerebellar granular layer of calpain-1 KO mice at PND7 (Figures 3A and 3C) and 10 (Figures 3B and 3C) but not 3 (Figure 3C), as compared to age-matched WT mice. Both the temporal and spatial patterns of neuronal apoptosis in calpain-1 KO mice were similar to those found in MK801-injected mice, suggesting that calpain-1 and NMDAR activate the same pro-survival pathway in developing CGCs. We determined the long-term consequences of enhanced CGC apoptosis in developing cerebellum by measuring CGC density in 3-month-old calpain-1 KO mice and WT mice. Calpain-1 KO mice had a small but significant reduction in CGC density, as compared to WT mice (Figure 3D).

In addition, we found enhanced apoptosis in multiple brain regions of calpain-1 KO mice at PND3 and 7 but not PND10, as compared to WT mice at the same ages (Figures S4A and S4B; Table S1), suggesting that calpain-1 activity also supports neuronal survival in multiple brain regions during postnatal development. NMDARs are transiently expressed and their activation also supports neuronal survival in the developing spinal cord (Brenneman et al., 1990; Kalb et al., 1992). However, we did not find increased apoptosis in the cervical or lumbar enlargement of spinal cord in MK801-injected mice or calpain-1 KO mice at PND7 (Figures S4C and S4D).

Calpain-1 KO Mice Exhibit Impaired Parallel Fiber to Purkinje Cell Synaptic Transmission

Calpain-1 KO mice exhibited normal overall cerebellar morphology (Figure S5A) and normal dendritic branching pattern (Figure S5B) of Purkinje cells. Golgi staining of cerebellar sections of 3-month-old WT and calpain-1 KO mice indicated that

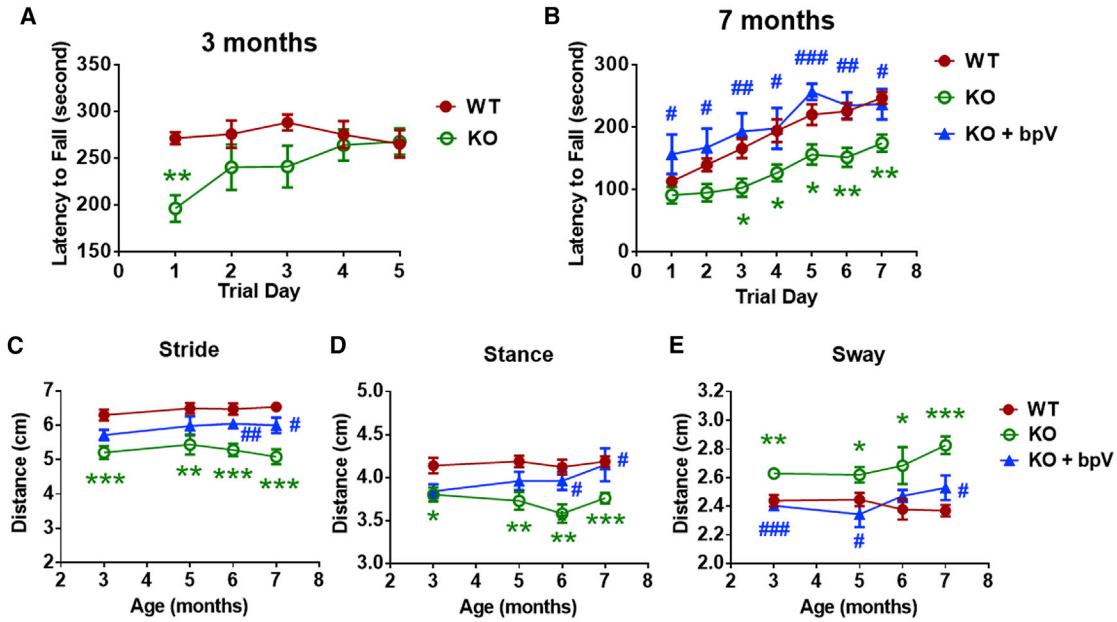

Figure 2. Impaired Motor Coordination in Adult Calpain-1 KO Mice Is Rescued by Postnatal bpV Treatment

(A) Rotarod test of WT and calpain-1 KO mice at 3 months of age. The latency to fall from an accelerating rotarod (from 4 to 40 rpm) was measured in three trials per day for 5 days. Results from the three trials on the same day were averaged. Each value represents mean ± SEM. n = 5–9. **p < 0.01 WT versus KO. Unpaired two-tailed t test.

(B) Rotarod test of WT, calpain-1 KO, and bpV-injected KO mice at 7 months of age. Saline or bpV (0.5 mg/kg) was injected (i.p.) twice per day to calpain-1 KO mice from postnatal day (PND) 1 to 7. The latency to fall from an accelerating rotarod (from 4 to 40 rpm) was measured in three trials per day for 7 days. Values for the three trials on the same day were averaged. Each value represents means ± SEM n = 9–14. *p < 0.05, **p < 0.01 WT versus KO. #p < 0.05, ##p < 0.01 KO versus KO + bpV. One-way ANOVA followed by Bonferroni test.

(C–E) Stride, stance, and sway lengths of WT, KO, and bpV-injected KO mice at 3–7 months of age. Results represent means ± SEM n = 9–14. *p < 0.05, **p < 0.01, ***p < 0.001 WT versus KO. #p < 0.05, ###p < 0.001 KO versus KO + bpV. One-way ANOVA followed by Bonferroni test.

spine density was comparable between WT and KO mice, but spine morphology was significantly different (Figures 3E–3G). Purkinje cells in KO mice had more thin or filopodia-like spines and less mushroom or stubby spines, as compared to WT mice, indicating that there is a higher proportion of immature spines in Purkinje cells of adult calpain-1 KO mice, as compared to WT mice.

The reduced CGC density and abnormal dendritic spine morphology of Purkinje cells led us to examine parallel fiber to Purkinje cell (PF-PC) synapses in KO mice. We first performed double immunostaining with a PF-specific presynaptic marker, VGluT1, and a postsynaptic marker, GluR2, in cerebellar sections of 3-month-old WT and calpain-1 KO mice (left and middle panel of Figure 4A). Both GluR2 and VGluT1 exhibited a puncta distribution in the molecular layer and the numbers of GluR2 and VGluT1 puncta were significantly reduced in the molecular layer of calpain-1 KO mice, as compared to WT mice (Figures 4B and 4C). The number of double-stained puncta, which correspond to PF-PC synapses, was also significantly reduced in KO mice (Figure 4D). While GluR2 and PSD95 levels in whole homogenates were comparable between WT and KO mice, they were significantly reduced in PSD fractions from KO mice (Figures 4E and 4F).

We recorded excitatory postsynaptic potentials (EPSPs) elicited in the Purkinje cell body layer by electrical stimulation of the parallel fibers at various stimulation intensities. This stimulation elicited a typical P1-N1-P2-N2 waveform (Barnes et al., 2011), where N1 corresponds to the presynaptic fiber volley and N2 to the postsynaptic population spike (Figure 4G). Responses elicited by stimulation intensity below 120 μA were too unreliable to be analyzed and only responses elicited by stimulation intensities above 120 μA were analyzed by calculating the ratio of N2 over N1, which reflects the efficiency of synaptic transmission. At all intensities, the N2/N1 ratio was smaller in KO as compared to WT mice and the overall difference between the two genotypes was statistically significant (Figure 4G).

Climbing fiber to Purkinje cell (CF-PC) synapses were double immunostained with a CF-specific presynaptic marker, VGluT2, and a Purkinje dendritic marker, calbindin, in cerebellar sections of WT and calpain-1 KO mice (Figure 4H). The densities of VGluT2 puncta were comparable between WT and KO mice (Figure 4I), suggesting that the CF-PC synapses were normal in calpain-1 KO mice.

Calpain-1-Dependent PHLPP1 Degradation and Akt Activation Are Deficient in Developing Cerebellum of Calpain-1 KO Mice

Calpain-1-mediated pro-survival pathway involves calpain-1 cleavage of PHLPP1 and subsequent Akt activation (Wang et al., 2013). Basal levels of PHLPP1, pAkt, and total Akt were

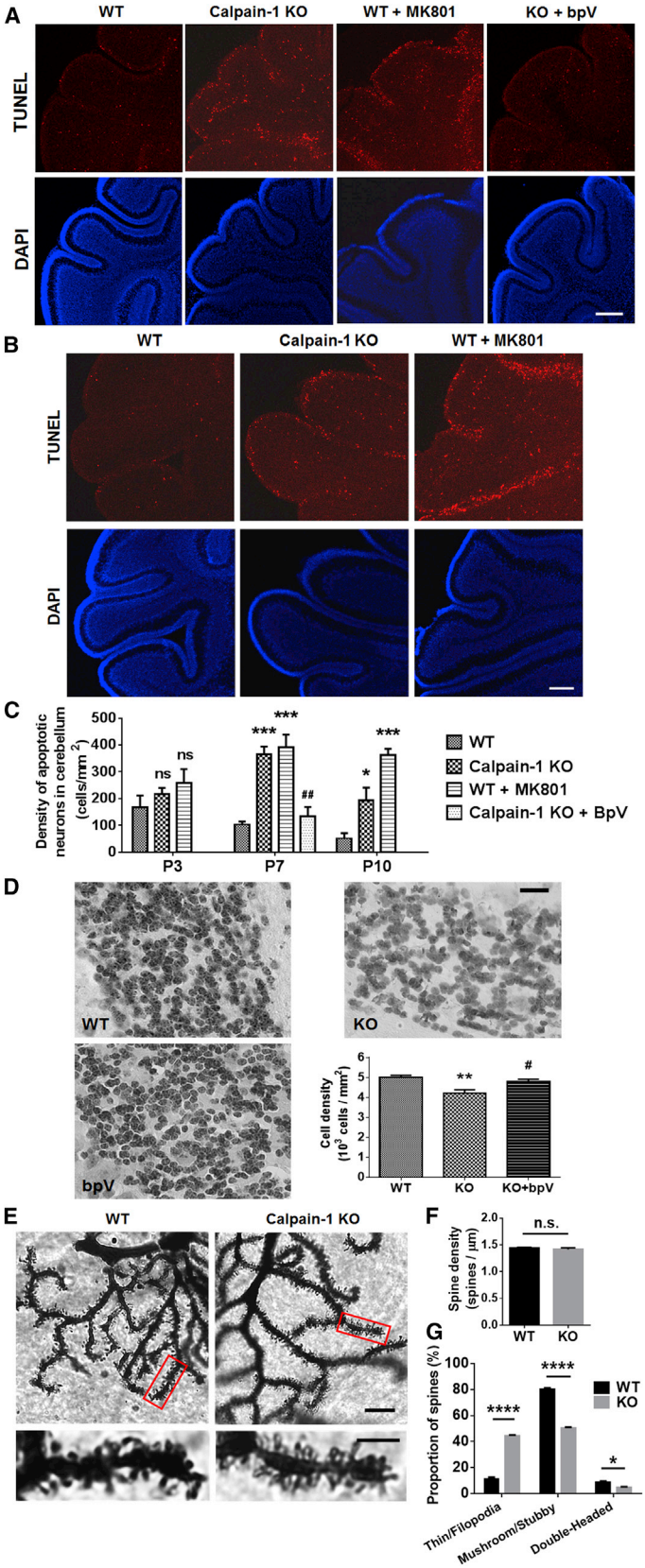

Figure 3. Increased Apoptosis during Postnatal Development and Decreased Density in Adult of Cerebellar Granule Cells in Calpain-1 KO Mice

(A) TUNEL staining in cerebellar sections shows increased apoptosis in cerebellum of PND7 calpain-1 KO mice and MK801-injected WT mice (i.p. injection, 0.5 mg/kg at 24, 16, and 8 hr before PND7), as compared to WT and bpV-injected KO mice at the same ages. Scale bar, 200 μm.

(B) Increased apoptosis in cerebellum of PND10 calpain-1 KO mice and MK801-injected WT mice (i.p. injection, 0.5 mg/kg at 24, 16, and 8 hr before PND10), as compared to WT mice. Scale bar, 200 μm.

(C) Number of apoptotic cells in cerebellum of WT, calpain-1 KO, MK801-injected WT, and bpV-injected KO mice at different postnatal days. Apoptotic cell densities in various sections from the same cerebellum were averaged (see Experimental Procedures). Results represent means ± SEM n = 4 (24 sections from four animals in each group). ns, no significant difference versus WT. *$p < 0.05$, ***$p < 0.001$ versus WT. ##$p < 0.01$ versus calpain-1 KO. One-way ANOVA followed by Bonferroni test.

(D) CGC density in 3-month-old calpain-1 KO mice is significantly lower, as compared to WT and bpV-injected KO mice at the same age. Scale bar, 20 μm. Cell densities of sections in the same cerebellum were then averaged (see Experimental Procedures for details). Results represent means ± SEM n = 5. **$p < 0.01$ versus WT. #$p < 0.05$ versus KO. One-way ANOVA followed by Bonferroni test.

(E) Golgi stained Purkinje cell dendrites and spines in 3-month-old calpain-1 KO and WT mice. Scale bar, 10 μm and 4 μm for magnified images.

(F) Dendritic spine densities were analyzed as spine count over length of dendrite. n = 3 (animals) for each genotype. 12–16 sections per animal were analyzed. Distal dendritic branches between 10 and 20 μm in length were measured and averaged for a slice mean. n.s., no significant difference between the groups. Two-tailed t test. Means ± SEM.

(G) Spine morphology. Calpain-1 KO mice had significantly more thin/filopodia and less mushroom/stubby and double-headed spines as compared to WT. n = 3 (animals) for each genotype. 9–16 slices per animal were analyzed. *$p < 0.05$, ****$p < 0.0001$ WT versus KO. Two-way ANOVA followed by Bonferroni test. Means ± SEM.

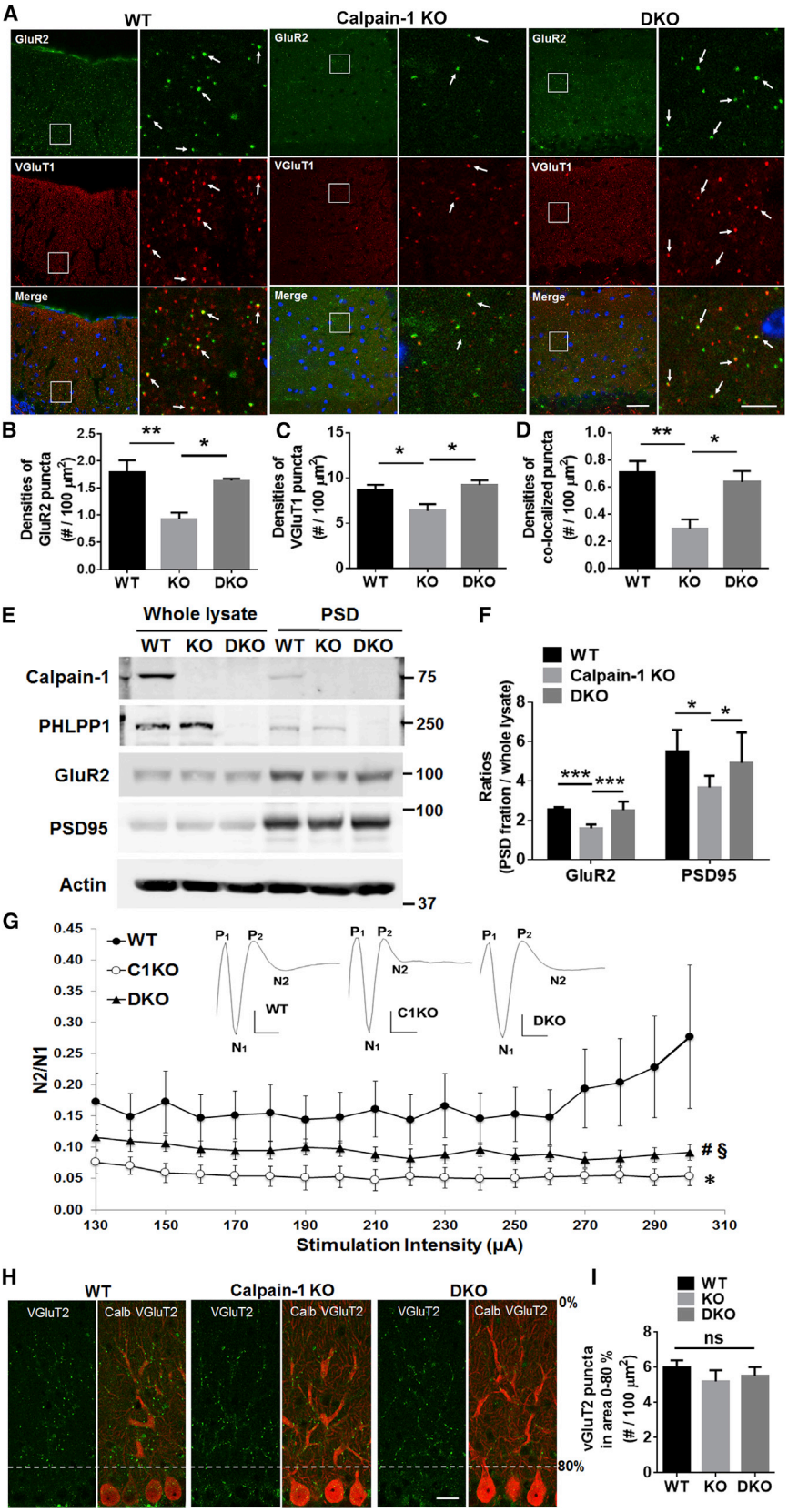

Figure 4. Reduced Synapse Number and Evoked Population Spike in Parallel Fiber to Purkinje Cell Synapses in Calpain-1 KO Mice Are Reversed in DKO Mice

(A) Co-staining of GluR2 and VGluT1 in cerebellar sagittal sections of 3-month-old WT (C57Bl/6), calpain-1 KO (C57Bl/6 × C57/SV129), and DKO mice (C57Bl/6 × C57/SV129). Scale bar, 40 and 10 μm for magnified images.

(B–D) Densities of GluR2 puncta, VGluT1 puncta and co-localized puncta in cerebellum of WT, calpain-1 KO, and DKO mice. Means ± SEM of six animals for WT and KO and four animals for DKO. *$p < 0.05$, **$p < 0.01$. One-way ANOVA followed by Bonferroni test.

(E) Levels of calpain-1, PHLPP1, GluR2, PSD95, and actin in whole lysates and PSD fractions of cerebellar homogenates from 3-month-old WT, calpain-1 KO, and DKO mice.

(F) Ratios of protein levels in PSD fractions to that in whole lysates in cerebellar homogenates of WT, calpain-1 KO, and DKO mice. n = 4–5 (animals). *$p < 0.05$, ***$p < 0.001$. One-way ANOVA followed by Bonferroni test. Means ± SEM.

(G) Parallel fibers to Purkinje cell EPSPs are reduced in calpain-1 KO mice, and partially restored in DKO mice. Acute cerebellar slices were prepared as described in Experimental Procedures, and field EPSPs were evoked by parallel fiber stimulation recorded in the Purkinje cell layer. Results were calculated as ratios of N2 over N1 and represent means ± SEM of ten to 11 slices from three to five mice. *$p < 0.001$, as compared to WT (univariate ANOVA followed by Bonferroni test); #$p < 0.001$, as compared to WT (univariate ANOVA followed by Bonferroni test); §$p < 0.001$, as compared to DKO (univariate ANOVA followed by Bonferroni test).

(H) Co-immunostaining of VGluT2 (green) and Calbindin (red) in cerebellar sections of 3-month-old WT, calpain-1 KO, and DKO mice. Scale bar, 20 μm.

(I) VGluT2 puncta densities in area 0%–80% (excluding cell body layer) of Purkinje cells in cerebellum of WT, KO, and DKO mice. Means ± SEM of four animals. ns, no significant difference. One-way ANOVA.

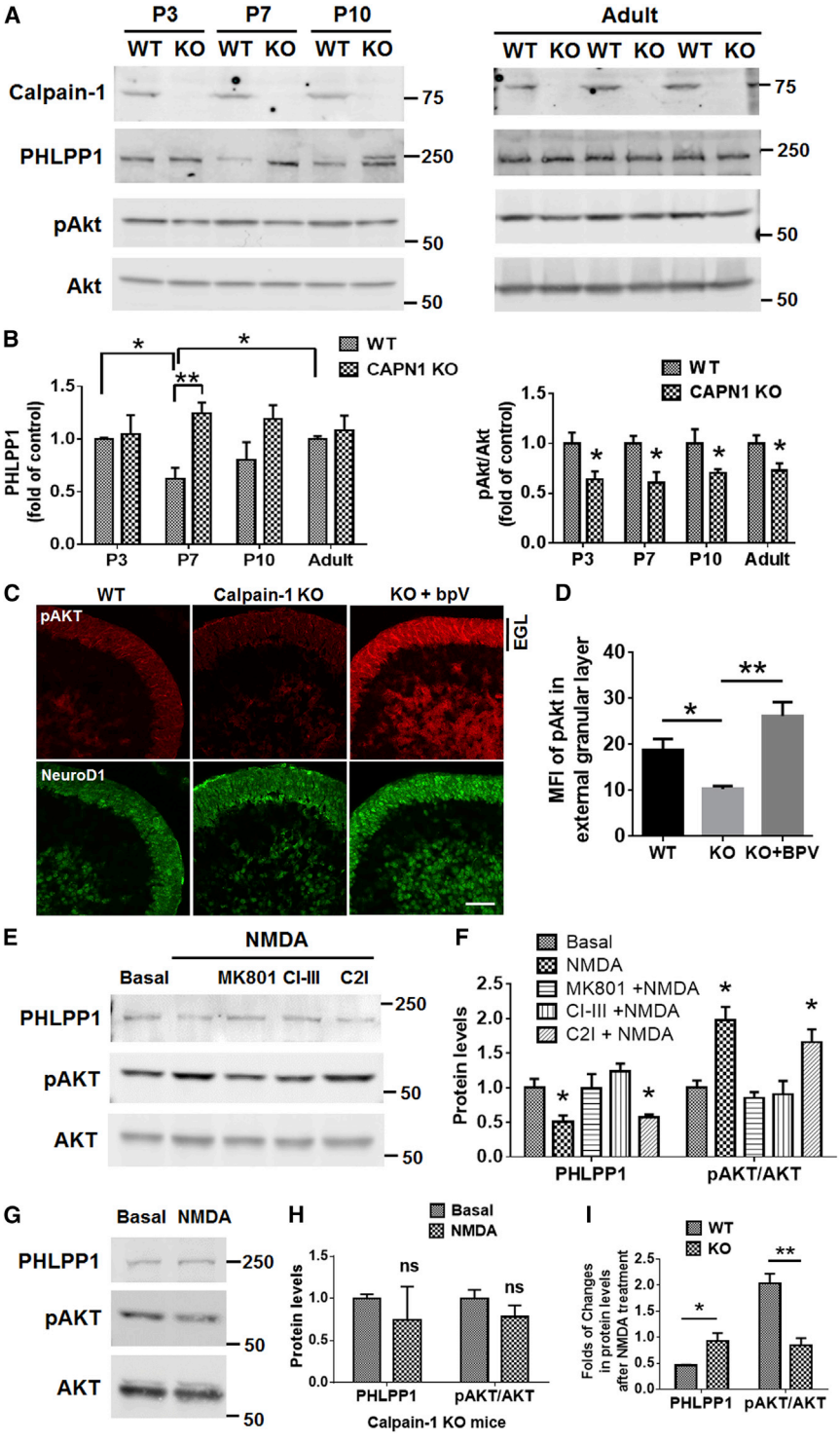

Figure 5. Increased PHLPP1 and Decreased Phospho-Akt Levels in Developing Cerebellum of Calpain-1 KO Mice

(A) Levels of PHLPP1, pAkt, and Akt in cerebellar homogenates of WT and calpain-1 KO mice, at PND3, 7, and 10 and 3 months (adult).

(B) Ratios of PHLPP1 to Akt and pAkt to Akt in cerebellum of WT and calpain-1 KO mice. Results represent means ± SEM n = 4–5. *p < 0.05, **p < 0.01. Two-way ANOVA followed by Bonferroni test.

(C) pAkt and NeuroD1 co-immunostaining in cerebellum of WT, calpain-1 KO, and bpV-injected KO mice at PND7. BpV (0.5 mg/kg) was injected (i.p.) 2 hr before perfusion. EGL, external granular layer. Scale bar, 40 μm.

(D) Mean fluorescence density (MFI) of pAkt signal in the external granular layer of cerebellum in WT, KO and bpV-injected KO mice at PND7. Means ± SEM of 4 animals. *p < 0.05, **p < 0.01. One-way ANOVA followed by Bonferroni test.

(E) Levels of PHLPP1 and pAkt levels 20 min after NMDA treatment (10 μM) of acute cerebellar slices from PND7 WT mice and effects of pretreatment with MK801 (50 μM), calpain inhibitor III (10 μM), and calpain-2 selective inhibitor (200 nM).

(F) Ratios of PHLPP1 to Akt, and pAkt to Akt, in each group. Results represent means ± SEM n = 3–4. *p < 0.05 versus basal group. One-way ANOVA followed by Bonferroni test.

(G) Effect of NMDA treatment of acute cerebellar slices from PND7 calpain-1 KO mice on PHLPP1 or pAkt.

(H) Ratios of pAkt to Akt and PHLPP1 to Akt in each group. Results represent means ± SEM n = 4. ns, no significant difference. Two-tailed t test.

(I) Ratios of protein levels after NMDA treatment to those under basal condition in cerebellar slices from PND7 WT and KO mice. n = 4. *p < 0.05, **p < 0.01. Two-way ANOVA followed by Bonferroni test.

measured in cerebellar homogenates of WT and calpain-1 KO mice at PND3, 7, 10, and 3 months (adult). PHLPP1 levels were lower in WT than in calpain-1 KO mice at all tested ages, although the decrease was statistically significantly only at PND7 levels (Figures 5A and 5B). PHLPP1 were also significantly lower at PND7 as compared toPND3 and adult, reflecting the increase in calpain-1 activity during this postnatal period. The decrease in PHLPP1 levels was not observed in calpain-1 KO mice at PND7 (P7 WT versus P7 KO, Figure 5B). Reflecting the higher levels of PHLPP1 in calpain-1 KO mice, levels of pAkt were lower in cerebellum of calpain-1 KO mice at all tested time points, including adult, as compared to age-matched WT mice (Figures 5A and 5B). Cerebellar sections from WT and KO mice at PND7 were double immunostained with pAkt and NeuroD1, a CGC marker. Immunoreactivity for pAkt was significantly lower in the external granular layer (EGL) of KO mice (Figures 5C and 5D).

Acute cerebellar slices of PND7 WT mice were treated with NMDA (10 μM) for 20 min. PHLPP1 levels were significantly decreased and pAkt levels increased after NMDA treatment.

Pretreatment with MK801 (50 μM) or calpain inhibitor III (10 μM) 10 min before NMDA treatment completely blocked NMDA-induced changes in PHLPP1 and pAkt (Figures 5E and 5F), but pretreatment with a selective calpain-2 inhibitor had no effect (Figures 5E and 5F), suggesting that calpain-2 activation was not involved. Moreover, NMDA-induced degradation of PHLPP1 and pAkt increase were absent in cerebellar slices of calpain-1 KO mice at PND7 (Figures 5G–5I), indicating that calpain-1 is required for NMDAR-mediated regulation of Akt in developing cerebellum.

Cerebellar Granule Cell Loss and Motor Deficits in Calpain-1 KO Mice Are Reversed by Activating Akt during the Critical Period of Development

To reverse reduced pAkt levels in cerebellum of calpain-1 KO mice during the early postnatal period, we treated calpain-1 KO mice from PND1 to PND7 with a PTEN inhibitor, bisperoxovanadium (bpV) (0.5 mg/kg, ip, twice daily), which has been shown to activate Akt (Boda et al., 2014; Li et al., 2009; Mao et al., 2013). BpV injection significantly increased pAkt levels in cerebellum of developing KO mice, as shown by both immunoblotting (Figures S6A and S6B) and immunostaining (Figures 5C and 5D), and completely prevented enhanced apoptosis in cerebellum (Figures 3A and 3C) and cerebrum (Table S1) of calpain-1 KO mice at PND7. Three months after bpV injection in KO mice, pAkt levels in cerebellum were reduced to the same levels as those found in control KO mice (Figures S6C and S6D), indicating that the effect of bpV on Akt was transient. However, the decrease in CGC density observed in 3-month-old KO mice was reversed by postnatal bpV injection (Figure 3D). Furthermore, the deficit in the rotarod test in 7-month-old KO mice was also completely reversed (Figure 2B), and the abnormal gait at different ages was partially or totally corrected (Figures 2C–2E) by postnatal bpV treatment. The above results indicate that reduced pAkt levels in developing cerebellum are responsible for the CGC loss and motor deficits observed in adult calpain-1 KO mice.

Calpain-1/PHLPP1 Double-Knockout Mice Have Normal CGC Density, PF-PC Transmission, and Motor Performance

To determine whether calpain-1 cleavage of PHLPP1 was essential for CGC survival, we generated double-KO mice, lacking both calpain-1 and PHLPP1 (DKO), as PHLPP1 KO should mimic calpain-1 cleavage of PHLPP1 and reverse the deficits caused by calpain-1 KO. Levels of pAkt were increased in cerebellar homogenates of DKO mice at PND7, as compared to calpain-1 KO mice (Figures 6A and 6B). The number of apoptotic neurons in cerebellum of PND7 DKO mice was significantly reduced and was comparable to that in control WT and PHLPP1 KO mice (Figures 6C and 6D). Consequently, CGC density in 3-month-old DKO mice was significantly increased, as compared to calpain-1 KO mice, and was similar to the value found in WT mice (Figures 6E and 6F).

The numbers of GluR2 puncta, VGluT1 puncta, and double-stained puncta in the molecular layer of 3-month-old DKO mice were significantly increased as compared to calpain-1 KO mice and were comparable to those of WT mice (Figures 4A–4D). Similarly, levels of GluR2 and PSD95 in the PSD fraction of DKO mice were significantly increased (Figures 4E and 4F). In addition, the N2/N1 ratios of the EPSPs recorded in cerebellar slices from DKO at all stimulation intensities were intermediate between those in WT and KO mice, indicating that synaptic transmission was at least partially restored in cerebellum of DKO mice (Figure 4G).

Finally, impaired rotarod performance and abnormal gait in calpain-1 KO mice were corrected in DKO mice. Calpain-1 KO mice with mixed background exhibited a significantly shorter latency to fall at trial days 6 and 7, as compared to age-matched WT mice. However, in DKO mice the latency to fall was significantly improved at trial days 6 and 7, as compared to calpain-1 KO mice (Figure 6G). The DKO mice also exhibited significantly longer strides and stances and shorter sways at 3, 4, and 5 months of age, as compared to calpain-1 KO mice with the same background (Figures 6H–6J). As a control, PHLPP1 KO mice exhibited normal rotarod performance and gaits, as compared to WT mice (Figures 6G–6J).

DISCUSSION

Our results indicate that null mutations or downregulation of calpain-1 leads to cerebellar ataxia in both humans and mice. Calpain-1 downregulation results in increased cerebellar PHLPP1 levels, which inhibit Akt and cause cerebellar granule cell death during a critical period of postnatal cerebellar development, and reduced granule cell density in adult KO mice. It also results in impaired spine morphology of Purkinje cells, with an increased proportion of immature spines, a decreased number of parallel fibers to Purkinje synapses and a decreased efficiency of synaptic transmission at these synapses. All these abnormalities are likely to contribute to the ataxia phenotype observed in mouse and humans. These abnormalities are reversed by either activating Akt during the critical period of cerebellar development (bpV treatment from P1 to P7), or downregulating PHLPP1, underscoring the critical role of calpain-1-mediated PHLPP1 truncation and Akt activation in postnatal development. Despite the fact that in the double knockout the deletions are systemic, all evidence indicates that the interactions take place within CGCs because both calpain-1 (Amadoro et al., 2007) and PHLPP1 (http://mouse.brain-map.org/gene/show/62602) are expressed in CGCs.

CAPN1 Is an Additional Gene for Spastic Ataxia

Cysteine 115 to tyrosine (C115Y) mutation of calpain-1 in the Parson Russell Terrier dog breed was associated with spinocerebellar ataxia (Forman et al., 2013). Cysteine 115 is in the catalytic site of calpain-1, and its mutation in recombinant human calpain-1 completely eliminated calpain-1 activity (Hata et al., 2013), indicating that the C115Y mutation in dog is a calpain-1-null mutation. In humans, we identified three consanguineous families that were homozygous in affected individuals around the *CAPN1* region and exome sequencing identified mutations in the *CAPN1* gene, and one recessive family with *CAPN1* compound heterozygous mutations. In one family, western blot and calpain assay in fibroblasts from the affected patient showed that calpain-1 expression and activity was absent,

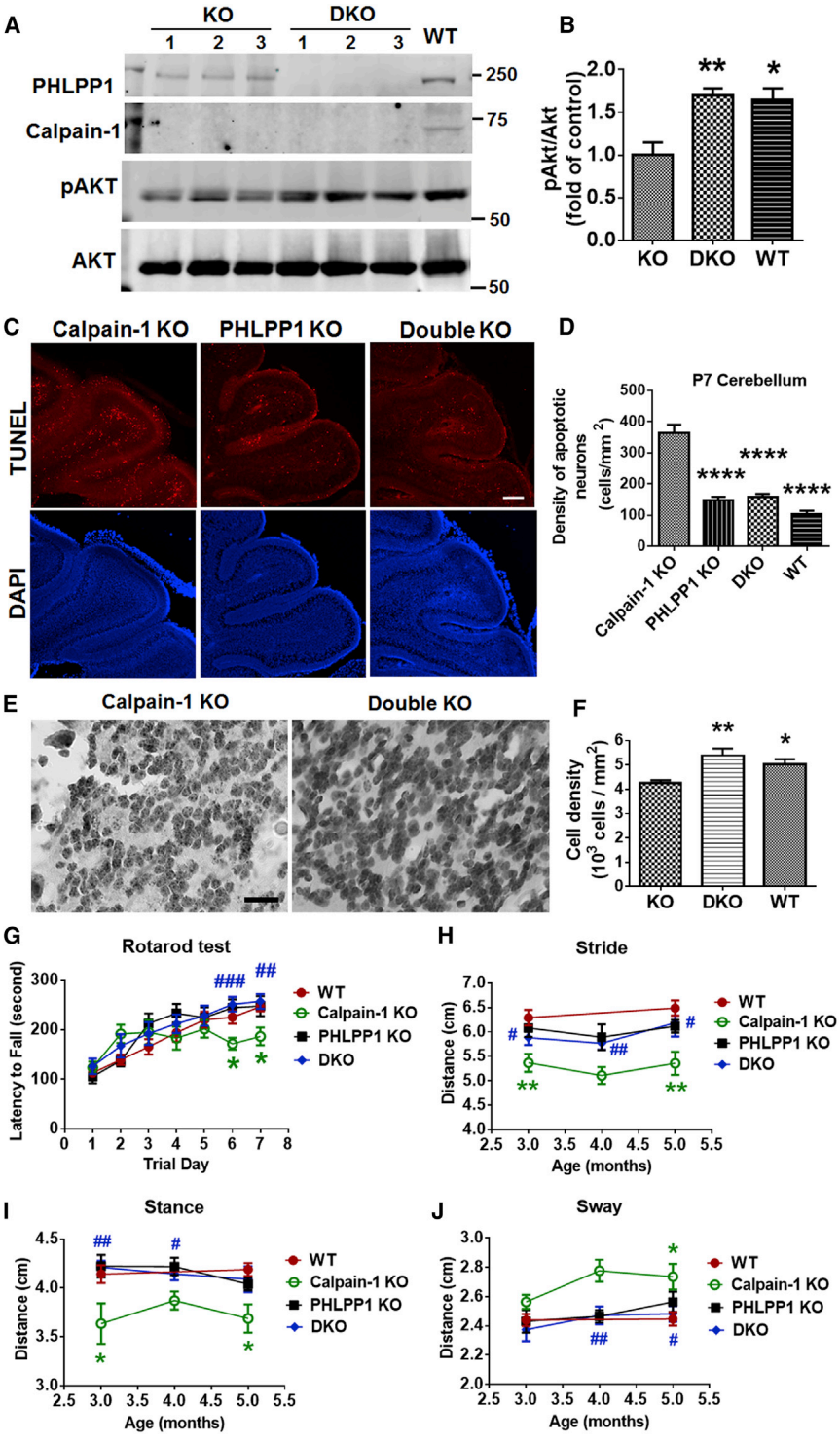

Figure 6. Calpain-1/PHLPP1 Double-Knockout Mice Have Increased pAkt Levels and Granule Cell Survival in Cerebellum, and Normal Motor Coordination, in Comparison to Calpain-1 KO Mice

(A) Levels of PHLPP1, calpain-1, pAKT, and AKT in cerebellum of three PND7 calpain-1 KO and DKO mice. A WT sample was included to show normal calpain-1 band.

(B) Ratios of pAkt to Akt in calpain-1 KO and DKO. Results represent means ± SEM n = 5. **p < 0.01 versus KO. Two-tailed t test.

(C) TUNEL staining in cerebellar sections of PND7 of Calpain-1 KO, PHLPP1 KO, and DKO mice. Scale bar, 200 μm.

(D) Density of apoptotic neurons in cerebellum of PND7 calpain-1 KO, PHLPP1 KO, DKO, and WT mice (C57Bl/6). Results represent means ± SEM n = 4 for WT and PHLPP1 KO, 5 for calpain-1 KO, 6 for DKO. ****p < 0.0001 versus KO. One-way ANOVA followed by Bonferroni test.

(E) H&E staining of CGCs in 3-month-old calpain-1 KO and DKO mice. Scale bar, 20 μm.

(F) CGC densities in 3-month-old WT, KO and DKO mice. Results represent means ± SEM n = 5. *p < 0.05, **p < 0.01 versus KO. One-way ANOVA followed by Bonferroni test.

(G) Rotarod test of WT, calpain-1 KO, PHLPP1 KO mice, and DKO mice at 7 months of age. The latency to fall represents means ± SEM n = 8–11. *p < 0.05 WT versus calpain-1 KO. ##p < 0.01, ###p < 0.001 calpain-1 KO versus DKO. One-way ANOVA followed by Bonferroni test.

(H–J) Stride, stance, and sway lengths of WT, calpain-1 KO, PHLPP1 KO, and DKO mice at 3, 4, and 5 months of age. Results represent means ± SEM n = 9–22. *p < 0.05, **p < 0.01 WT versus KO. #p < 0.05, ##p < 0.01, ###p < 0.001 KO versus DKO. One-way ANOVA followed by Bonferroni test.

indicating that this ataxia patient is a calpain-1 KO human. A second family harbored a homozygous frameshift variant, and the mutations in the other two families are predicted to produce functional inactivation of calpain-1. Thus, calpain-1 KO mice provide a rational model to study the mechanism underlying ataxia in dogs and humans. While calpain-1 KO mice exhibited an ataxia phenotype, which became more pronounced with age, as shown by rotarod and gait tests, the phenotype was not as severe as that observed in dogs and humans with calpain-1 mutations. While this raises the possibility that the alterations found in KO mice could explain only part of the basis for the ataxia in humans (and possibly dogs), it is not uncommon that mutation-related phenotypes in mice are less severe than those observed in humans, as in Atm-deficient mice (Barlow et al., 1996), which could reflect differences in temporal and spatial rates of development between mice and humans. It is nevertheless logical to assume that all the abnormalities found in KO mice contribute to the observed motor deficits in calpain-1 KO mice, as motor function was restored in bpV-injected KO mice and in DKO mice.

Increased calpain activity can also lead to ataxic phenotype. Thus, mutation in βIII spectrin in both human and mouse caused increased calpain proteolysis of αII spectrin, which results in ataxic and seizure phenotypes (Stankewich et al., 2010). In addition, enhanced calpain activity aggravated pathogenesis of spinocerebellar ataxia type 3 (SCA3) (Hübener et al., 2013). Together with our findings, those studies suggest that unbalanced calpain activity, either too little or too much, can result in cerebellar dysfunction and ataxia.

The NMDAR/Calpain-1/PHLLP1/Akt Pro-survival Pathway Limits the Extent of Neuronal Apoptosis in Developing Cerebellar Granule Cells

Our results clearly indicate that the NMDAR/calpain-1/PHLLP1/Akt pro-survival pathway, which we previously identified in cultured cortical neurons and acute hippocampal slices (Wang et al., 2013), is active in developing CGCs, where it limits the extent of CGC apoptosis. Several lines of evidence support this conclusion. First, basal levels of PHLPP1 were increased and those of pAkt decreased in fibroblasts of the patient with a calpain-1-null mutation. Similarly, increased PHLPP1 and decreased pAkt levels were found in cerebellar homogenates of calpain-1 KO mice, indicating that calpain-1 activity normally reduces PHLPP1 levels and maintains Akt activated during the postnatal period in cerebellum. Second, a decreased density of pAkt-positive puncta was found in cerebellar granular layer but not in Purkinje or molecular layer of calpain-1 KO mice, suggesting that calpain-1-dependent regulation of Akt only takes place in CGCs but not in other cerebellar cell types. Third, calpain-1 KO eliminated NMDA-triggered PHLPP1 cleavage and Akt activation in acute cerebellar slices, suggesting that calpain-1 is required for NMDAR-activity-dependent regulation of PHLPP1 and Akt. Fourth, lack of PHLPP1 restored normal levels of pAkt in developing cerebellum of calpain-1 KO mice, indicating that PHLPP1 is downstream of calpain-1 and that its level is important for Akt regulation. Finally, reduced Akt activity was associated with enhanced CGC apoptosis in calpain-1 KO mice, while increased Akt activity was associated with reduced CGC apoptosis in bpV-injected WT and in DKO mice.

NMDAR- and calpain-1-mediated neuronal survival during brain development was not limited to CGCs, as enhanced apoptosis was present in other brain regions such as cortex, striatum, and hippocampus in developing calpain-1 KO mice. Thus, we cannot rule out the possibility that enhanced neuronal death in other regions of the motor system, such as motor cortex and striatum, contributes to the motor impairment observed in calpain-1 KO mice, and possibly humans. Furthermore, the important roles of calpain-1 in hippocampal neuronal survival during development and in synaptic plasticity in adult (Wang et al., 2014; Zhu et al., 2015) may contribute to the cognitive decline found in ataxia patients with *CAPN1* mutations.

Calpain-1-Mediated Survival of Developing Cerebellar Granule Cells Is Required for Normal Density of Adult Cerebellar Granule Cells

Elimination of excessive neurons occurs during normal CNS development. During this process, NMDAR activity is required for neuronal survival, and only neurons establishing functional synaptic connections survive during development. This mechanism has been shown in various types of neurons, including CGCs (Ikonomidou et al., 1999; Monti et al., 2002). In CGCs, the period of NMDAR dependence is between PND7 and PND11 (Monti and Contestabile, 2000), which is consistent with our results showing that MK801 treatment enhanced CGC apoptosis at PND7 and PND10 but not PND3. Our results indicate that lack of calpain-1 produces the same pattern of enhanced apoptosis in developing cerebellum as MK801 treatment in WT mice. Enhanced apoptosis was found at PND7 and PND10 but not PND3, and most apoptosis occurred in the external and internal granular layer of cerebellum. Thus, NMDAR and calpain-1 are in the same signaling cascade required to support CGC survival. Enhanced apoptosis during postnatal development results in reduced CGC density in adult calpain-1 KO mice, which is consistent with the idea that CGC neurogenesis in mammalian cerebellum is strictly limited to the early postnatal period (Altman, 1972).

Despite reduced CGC density, calpain-1 KO mice exhibited normal overall Purkinje cell morphology (Figure S5B). However, careful analysis of Purkinje cell spine morphology indicated that calpain-1 KO resulted in immature spine morphology, reduced number of GluR2 subunits, reduced number of synaptic contacts, and reduced synaptic efficiency at PF-PC synapses. The reduced number of mature spines in Purkinje cells is likely due to a reduced number of PF-PC synapses, which was caused by impaired calpain-1-PHLPP1-Akt pathway and reduced CGC number in calpain-1 KO mice. Many previous publications showed similar examples in which either loss (Shmerling et al., 1998) or dysfunction (Chen et al., 1999; Hashimoto et al., 1999) of cerebellar granule cells leads to impaired PF-PC transmission and ataxia. In addition, we and another lab previously found that dysregulation of calpain or Akt affects actin polymerization, which is important for synapse formation and function and regulating the shape of the dendritic spines (Briz et al., 2015; Huang et al., 2013). We previously reported that calpain-1 activation was critical for induction of long-term potentiation (LTP) at hippocampal synapses (Wang et al., 2014), and it has been repeatedly proposed that establishment of synaptic contacts during the postnatal period might require a mechanism similar to LTP (Chaudhury et al., 2016). Thus, the absence of calpain-1 at the PF-PC synapses is likely to result in abnormal maturation of dendritic spines, and decreased synaptic efficiency of these synapses.

Enhanced neuronal apoptosis and reduced CGC density were completely reversed by restoring normal levels of phosphorylated Akt in cerebellum of calpain-1 KO mice with treatment with the phosphatase inhibitor bpV during the critical developing period. While the effect of bpV treatment on Akt activity was not permanent, the temporary rescue of Akt activation during development resulted in normal CGC density in adult, highlighting the importance of Akt regulation for CGC development. BpV is an inhibitor of the phosphatase that regulates Akt as well as other targets (Song et al., 2012). To rule out the possibility that the rescuing effect of bpV injection could be due to modifications of other PTEN targets, we generated calpain-1/PHLPP1 DKO mice. PHLPP1 KO rescued Akt activity and completely prevented CGC loss caused by calpain-1 KO, prevented the decrease in GluR2

subunits at PF-PC synapses, and partially reversed the decrease in synaptic efficiency at these synapse. Finally, it also reversed the abnormalities in motor function observed in calpain-1 KO mice. These results clearly indicate that PHLPP1, among other calpain-1 substrates, has a critical role in the normal development of CGCs and the PF-PC synapses.

Conclusions

Lack of calpain-1 or null mutations of calpain-1 are associated with cerebellar ataxia in mice and humans. Together with the previous report that a null mutation in dogs also presented with cerebellar ataxia, these findings identify *CAPN1* as a cerebellar ataxia gene. The identification of the underlying mechanism, abnormal development of CGCs and PF-PC synapses provides potential therapeutic treatment for this type of cerebellar ataxia. In addition, considering the role of calpain-1 in synaptic plasticity and learning and memory, these results establish a link between this type of cerebellar ataxia and cognitive deficits.

EXPERIMENTAL PROCEDURES

Animal use in all experiments followed NIH guidelines, and all protocols were approved by the Institution Animal Care and Use Committee of Western University of Health Sciences. Calpain-1 KO mice on a C57Bl/6 background were generously provided by Dr. Chishti (Tufts University). PHLPP1 KO mice on a C57/SV129 background were generously provided by Dr. Newton (UCSD). Calpain-1$^{-/-}$ mice were crossed with PHLPP1$^{-/-}$ to produce calpain-1$^{-/-}$ PHLPP1$^{-/-}$ (DKO) and calpain-1$^{-/-}$ PHLPP1$^{+/+}$ (control).

Gait Analysis

Mice were trained for 2 days to walk through the tunnel and then tested for two trials. Two to four steps from the middle portion of each run were analyzed for hind-stride length and hind-base width (distance between the right and left hind-limb strides, sway distance).

Rotarod Test

The experimental procedure was adapted from previously described procedures (Chen et al., 2009; Mulherkar and Jana, 2010; Sun et al., 2015a) using a rotarod apparatus (Med Associates). The total testing period lasted 8 days, 1 training day followed by 7 trial days. For day 1 training, the rotor was set at a constant speed of 4 rpm, and animals were placed on the rod for 30 s. If the animal fell off the rod prior to the end of the 30 s, they were placed back on the rod. This was repeated until the animal could maintain itself on the rod for the full 30-s duration. Trial days 1 through 7 consisted of three trials of 5 min each. The rod was set to ramp up from 4 to 40 rpm over the course of 5 min. The trial ended when the animal fell off the rod or at the end of 5 min, and the latency to fall was recorded in seconds. Trials were repeated three times per day with at least a 15-min rest period for each animal between trials. Data were expressed as the average time, in seconds (means ± SEM), of the latency to fall.

TUNEL Staining

TUNEL staining was performed in six sections at a 240-μm interval from each cerebellum or in eight sections at 1.54, 0.50, −0.58, −1.58, −1.94, −2.46, −2.92, and −3.88 Bregma from each cerebrum, using the ApopTag In Situ Apoptosis Detection Kit (S7165, Millipore), following the manufacturer's instructions. Sections were visualized under a confocal microscope (Nikon). For cerebellar analysis, the outline of the cerebellum in each image was drawn using "freehand selections" in ImageJ to exclude the surrounding area. TUNEL positive nuclei in cerebellar area were counted using "analyze particles" in ImageJ. Density of TUNEL positive nuclei per square millimeter of cerebellar area in each section was analyzed. Values of six sections in each cerebellum were averaged. Visualization and quantification were performed by a blind observer to avoid bias (see Supplemental Information for details).

H&E Staining and Cell Counting

H&E staining was performed on six sections (10 μm thick) at a 240-μm interval in each cerebellum, using Hematoxylin solution Harris modified (HHS32, Sigma) and Eosin Y solution aqueous (HT110232, Sigma). Cell numbers in a 150 × 150 μm^2 area in the intermediate stratum of the granular layer (Palkovits et al., 1971) in each folium were analyzed using ImageJ. Cell densities of all folia in each section were averaged. Cell densities of six sections in each cerebellum were then averaged to get the cell density of each cerebellum.

Acute Cerebellar Slice Preparation and Treatment

Cerebellar sagittal slices (400 μm thick) from PND7 WT or calpain-1 KO mice were prepared as previously described (Wang et al., 2014). After 1 hr recovery, cerebellar slices were incubated in 2 ml of freshly oxygenated artificial cerebrospinal fluid (aCSF) medium with 10 μM NMDA for 20 min.

Western Blot

Western blot analysis was performed as previously described (Wang et al., 2014). The primary antibodies used were calpain-1 (1:1,000, 2556, CST), calpain-2 (1:1,000, LS-B12657, LSBio), PHLPP1 (1:1,000, 07-1341, Millipore), phospho-Akt Ser473 (1:3,000, 4060, CST), and Akt (1:2,000, 2920).

Calpain Assay

The hydrolysis of the fluorogenic substrate Suc-Leu-Tyr-AMC by calpains in human fibroblast lysates was performed as previously described (Wang et al., 2014), with some modifications (see the Supplemental Information for details).

Immunohistochemistry

Immunohistochemistry was performed as previously described (Wang et al., 2014). The primary antibodies used were rabbit phospho-Akt (Ser473) antibody (1:100, 4060, CST), mouse NeuroD1 antibody (1:300, H00004760-M01, Novus Biologicals), rabbit calbindin antibody (1:500, 13176, CST) antibody, mouse GluR2 antibody (1:500, MAB397, EMD Millipore), rabbit VGluT1 antibody (1:500, ab104898, Abcam), and/or mouse VGluT2 antibody (1:300, MAB5504, EMD Millipore). For mean fluorescence density (MFI) analysis of pAkt signal in the cerebellum of PND7 mice, four sagittal sections at a 240-μm interval in each cerebellum were stained and analyzed. In each section, four 120 × 30 μm areas in external granular layer were analyzed. MFI value of pAkt signal in each area was acquired in ImageJ. Averaged MFI in four sections off each cerebellum was calculated.

For puncta analysis of GluR2 and VGluT1, four sagittal sections at a 240-μm interval in each cerebellum were stained and analyzed. In each section, four 160-×-80-μm areas in molecular layer were analyzed. The Red and Green Puncta Colocalization Macro in ImageJ were used to count GluR2, VGluT1, and co-localized puncta. Averaged densities of GluR2, VGluT1, and co-localized puncta (numbers per100 μm^2) in four sections of each cerebellum were calculated.

For puncta analysis of VGluT2, four sagittal sections at a 240-μm interval in each cerebellum were stained and analyzed. In each section, four 185-×-120-μm regions in Purkinje and molecular layer were analyzed. VGluT2 puncta in 0%–80% area (excluding cell body layer) of each region were counted by ImageJ. Averaged densities of VGluT2 puncta (numbers per 100 μm^2) in four sections of each cerebellum were calculated.

Dendritic Spine Analysis

Golgi impregnation was performed in the cerebellum of 3-month-old WT and calpain-1 KO mice according to FD Rapid GolgiStain Kit instructions (FD Neurotechnologies). 100-μm sagittal sections of the cerebellum were sliced. Images of dendritic branches of Purkinje cells were acquired using a Zeiss light microscope with a 60× objective. Using the Analyze Skeleton plugin of ImageJ software, spines densities were analyzed in random selected distal branches between 10 and 20 μm in length. Spine morphology analysis was performed as previously described with some changes (Miyoshi et al., 2014) (see the Supplemental Information).

Preparation of Postsynaptic Density Fraction

Preparation of postsynaptic density (PSD) fraction was performed as previously described (Sun et al., 2015b). Cerebellar cortex of the 3-month-old mouse

was homogenized in ice-cold HEPES-buffered sucrose solution (0.32 M sucrose, 4 mM HEPES [pH 7.4]) with protease inhibitor cocktail (78446, Thermo Fisher Scientific). Homogenates were centrifuged at 900 × *g* for 10 min to remove large debris (P1). The supernatant (S1) was then centrifuged at 11,000 × *g* for 20 min to obtain the crude synaptosomal (P2) and cytosolic (S2) fractions. The PSD-enriched fraction (P3) was obtained by incubating P2 pellets in HEPES-buffered sucrose solution plus 0.5% Triton X-100 on ice for 20 min and then centrifuging at 32,000 × *g* for 1 hr. Final pellets were sonicated in resuspension buffer (10 mM Tris [pH 8], 1 mM EDTA, and 1% SDS). Protein concentrations were determined with a BCA protein assay kit (Pierce). Same amount of proteins from the S1 fraction and PSD fractions were resolved by SDS-PAGE and immunoblotted with the indicated antibodies.

Electrophysiology in Acute Cerebellar Slice

Acute cerebellar coronal slices (350 μm) were prepared, and field EPSPs were evoked by parallel fiber stimulation recorded in the Purkinje cell layer, as previously described (Barnes et al., 2011). Population spikes were recorded by a differential amplifier (DAM 50, World Precision Instruments; 10 kHz high- and 300 Hz low-cutoff filter; gain = 1,000) and sampled at 10 kHz on Clampex. A dissecting microscope was used for visualizing the slices in the recording chamber, and recording and stimulating electrodes were randomly tested on the vermal part of the cerebellar slice with a test pulse of 130 μA until a characteristic P_1-N_1-P_2-N_2 waveform, as reported in Barnes et al. (2011) was found. The absolute values of the ratios between the amplitude of N_2 and N_1 at different stimulation intensities (10–300 μA) were analyzed.

Patients

Autosomal recessive families of Tunisian, Bangladeshi, or European origin were studied (pedigrees shown in Figures 1 and S1–S3). All families have a clinically similar ataxia. All individuals gave informed consent. The work was approved by the Office of Human Subjects Research at the NIH and the University College London Hospitals ethics committee (approval no. 06/N076) or Paris Necker ethics committee (RBM 01-29 and RBM 03-48 to A.D. and A.B.).

Genetic Linkage/Homozygosity Analysis

Family members were genotyped using Illumina CytoSNP12 arrays with 301,232 genome-wide markers, and the raw data were processed in GenomeStudio (Illumina). Genotypes were examined with the use of a multipoint parametric linkage analysis and haplotype reconstruction performed with Simwalk2 (Sobel et al., 2001).

Exome Sequencing

Libraries were prepared using the TruSeq DNA sample prep kit (Illumina) and 1 μg of patient DNA. Fragmentation was performed with the Covaris shearing system using the 300-bp with size selection by excision from the area between 300 and 400 bp on an agarose gel.

CAPN1 Sanger Sequencing

To validate the results of exome sequencing and screen controls, primers were designed using Primer3 to amplify the entire *CAPN1* gene (primers available on request). Clean PCR product was sequenced using BigDye Terminator 3.1 chemistry (Life Technologies) and cleaned with Millipore filter plates prior to capillary electrophoresis on an ABI 3130XL Genetic Analyzer (ABI Biosystems).

Statistical Analyses

In all cases, error bars indicate SEM. N values represent numbers of animals tested. To compute p values, unpaired Student's t test, one-way ANOVA, and two-way ANOVA followed by Bonferroni test were used, as indicated in the figure legends.

SUPPLEMENTAL INFORMATION

Supplemental Information includes Supplemental Experimental Procedures, six figures, and one table and can be found with this article online at http://dx.doi.org/10.1016/j.celrep.2016.05.044.

AUTHOR CONTRIBUTIONS

Y.W. performed the majority of the experiments, prepared the figures, and wrote the manuscript. J.H. performed the human gene analysis. D.L. performed a number of experiments. M.H. performed the human gene analysis. Y.L. performed the behavioral experiments. K.-H.L. performed the electrophysiological experiments. V.P. and J.S. performed a number of experiments. F.H. and R.A. provided clinical details. S.W. performed human gene analysis. J.S., N.B., J.T., and A.B.S. performed a number of experiments. X.B. designed experiments and wrote the manuscript. M.C. performed human gene analysis and wrote the manuscript. A.B., G.S., and A.D. performed human gene analysis. H.H. designed human experiments, analyzed results, and wrote the manuscript. M.B. designed the studies and wrote the manuscript.

ACKNOWLEDGMENTS

This work was supported by grant P01NS045260-01 from NINDS (PI: Dr. C.M. Gall), the Medical Research Council UK, Brain Research Trust, Wellcome Trust, NIHR UCL/UCLH BRC, the Agence Nationale de la Recherche (ANR; to G.S.), the Verum Foundation (to G.S. and A.B.), the patient association Connaitre les Syndromes Cérébelleux (CSC; to G.S.), the Roger de Spoelberg Foundation (to A.B.), and the European Union (Omics call: NEUROMICS, to A.B. and A.D.) and benefited from the program Investissements d'avenir ANR-10-IAIHU-06 (to the ICM Institute). The authors want to thank Western University of Health Sciences for the financial support to M.B. X.B. is also supported by funds from the Daljit and Elaine Sarkaria Chair. M.C. was the recipient of a fellowship from the Fond National de la Recherche Scientifique (aspirant FNRS). The authors are grateful to Claire Sophie Davoine and to the DNA and cell biobank of the ICM institute for their technical assistance.

Received: July 24, 2015
Revised: April 14, 2016
Accepted: May 10, 2016
Published: June 16, 2016

REFERENCES

Altman, J. (1972). Postnatal development of the cerebellar cortex in the rat. 3. Maturation of the components of the granular layer. J. Comp. Neurol. *145*, 465–513.

Amadoro, G., Pieri, M., Ciotti, M.T., Carunchio, I., Canu, N., Calissano, P., Zona, C., and Severini, C. (2007). Substance P provides neuroprotection in cerebellar granule cells through Akt and MAPK/Erk activation: evidence for the involvement of the delayed rectifier potassium current. Neuropharmacology *52*, 1366–1377.

Arias, E., Koga, H., Diaz, A., Mocholi, E., Patel, B., and Cuervo, A.M. (2015). Lysosomal mTORC2/PHLPP1/Akt regulate chaperone-mediated autophagy. Mol. Cell *59*, 270–284.

Balázs, R., Jørgensen, O.S., and Hack, N. (1988). N-methyl-D-aspartate promotes the survival of cerebellar granule cells in culture. Neuroscience *27*, 437–451.

Barlow, C., Hirotsune, S., Paylor, R., Liyanage, M., Eckhaus, M., Collins, F., Shiloh, Y., Crawley, J.N., Ried, T., Tagle, D., and Wynshaw-Boris, A. (1996). Atm-deficient mice: a paradigm of ataxia telangiectasia. Cell *86*, 159–171.

Barnes, J.A., Ebner, B.A., Duvick, L.A., Gao, W., Chen, G., Orr, H.T., and Ebner, T.J. (2011). Abnormalities in the climbing fiber-Purkinje cell circuitry contribute to neuronal dysfunction in ATXN1[82Q] mice. J. Neurosci. *31*, 12778–12789.

Baudry, M., Simonson, L., Dubrin, R., and Lynch, G. (1986). A comparative study of soluble calcium-dependent proteolytic activity in brain. J. Neurobiol. *17*, 15–28.

Boda, B., Mendez, P., Boury-Jamot, B., Magara, F., and Muller, D. (2014). Reversal of activity-mediated spine dynamics and learning impairment in a mouse model of Fragile X syndrome. Eur. J. Neurosci. *39*, 1130–1137.

Brenneman, D.E., Forsythe, I.D., Nicol, T., and Nelson, P.G. (1990). N-methyl-D-aspartate receptors influence neuronal survival in developing spinal cord cultures. Brain Res. Dev. Brain Res. *51*, 63–68.

Briz, V., Zhu, G., Wang, Y., Liu, Y., Avetisyan, M., Bi, X., and Baudry, M. (2015). Activity-dependent rapid local RhoA synthesis is required for hippocampal synaptic plasticity. J. Neurosci. *35*, 2269–2282.

Chaudhury, S., Sharma, V., Kumar, V., Nag, T.C., and Wadhwa, S. (2016). Activity-dependent synaptic plasticity modulates the critical phase of brain development. Brain Dev. *38*, 355–363.

Chen, L., Bao, S., Qiao, X., and Thompson, R.F. (1999). Impaired cerebellar synapse maturation in waggler, a mutant mouse with a disrupted neuronal calcium channel gamma subunit. Proc. Natl. Acad. Sci. USA *96*, 12132–12137.

Chen, Q., Peto, C.A., Shelton, G.D., Mizisin, A., Sawchenko, P.E., and Schubert, D. (2009). Loss of modifier of cell adhesion reveals a pathway leading to axonal degeneration. J. Neurosci. *29*, 118–130.

Chen, M., Pratt, C.P., Zeeman, M.E., Schultz, N., Taylor, B.S., O'Neill, A., Castillo-Martin, M., Nowak, D.G., Naguib, A., Grace, D.M., et al. (2011). Identification of PHLPP1 as a tumor suppressor reveals the role of feedback activation in PTEN-mutant prostate cancer progression. Cancer Cell *20*, 173–186.

Du, K., and Montminy, M. (1998). CREB is a regulatory target for the protein kinase Akt/PKB. J. Biol. Chem. *273*, 32377–32379.

Forman, O.P., De Risio, L., and Mellersh, C.S. (2013). Missense mutation in CAPN1 is associated with spinocerebellar ataxia in the Parson Russell Terrier dog breed. PLoS ONE *8*, e64627.

Hamakubo, T., Kannagi, R., Murachi, T., and Matus, A. (1986). Distribution of calpains I and II in rat brain. J. Neurosci. *6*, 3103–3111.

Hashimoto, K., Fukaya, M., Qiao, X., Sakimura, K., Watanabe, M., and Kano, M. (1999). Impairment of AMPA receptor function in cerebellar granule cells of ataxic mutant mouse stargazer. J. Neurosci. *19*, 6027–6036.

Hata, S., Kitamura, F., and Sorimachi, H. (2013). Efficient expression and purification of recombinant human μ-calpain using an Escherichia coli expression system. Genes Cells *18*, 753–763.

Huang, W., Zhu, P.J., Zhang, S., Zhou, H., Stoica, L., Galiano, M., Krnjević, K., Roman, G., and Costa-Mattioli, M. (2013). mTORC2 controls actin polymerization required for consolidation of long-term memory. Nat. Neurosci. *16*, 441–448.

Hübener, J., Weber, J.J., Richter, C., Honold, L., Weiss, A., Murad, F., Breuer, P., Wüllner, U., Bellstedt, P., Paquet-Durand, F., et al. (2013). Calpain-mediated ataxin-3 cleavage in the molecular pathogenesis of spinocerebellar ataxia type 3 (SCA3). Hum. Mol. Genet. *22*, 508–518.

Ikonomidou, C., Bosch, F., Miksa, M., Bittigau, P., Vöckler, J., Dikranian, K., Tenkova, T.I., Stefovska, V., Turski, L., and Olney, J.W. (1999). Blockade of NMDA receptors and apoptotic neurodegeneration in the developing brain. Science *283*, 70–74.

Kalb, R.G., Lidow, M.S., Halsted, M.J., and Hockfield, S. (1992). N-methyl-D-aspartate receptors are transiently expressed in the developing spinal cord ventral horn. Proc. Natl. Acad. Sci. USA *89*, 8502–8506.

Kim, J.C., Cook, M.N., Carey, M.R., Shen, C., Regehr, W.G., and Dymecki, S.M. (2009). Linking genetically defined neurons to behavior through a broadly applicable silencing allele. Neuron *63*, 305–315.

Li, D., Qu, Y., Mao, M., Zhang, X., Li, J., Ferriero, D., and Mu, D. (2009). Involvement of the PTEN-AKT-FOXO3a pathway in neuronal apoptosis in developing rat brain after hypoxia-ischemia. J. Cereb. Blood Flow Metab. *29*, 1903–1913.

Liu, J., Liu, M.C., and Wang, K.K. (2008). Calpain in the CNS: from synaptic function to neurotoxicity. Sci. Signal. *1*, re1.

Mao, L., Jia, J., Zhou, X., Xiao, Y., Wang, Y., Mao, X., Zhen, X., Guan, Y., Alkayed, N.J., and Cheng, J. (2013). Delayed administration of a PTEN inhibitor BPV improves functional recovery after experimental stroke. Neuroscience *231*, 272–281.

Masubuchi, S., Gao, T., O'Neill, A., Eckel-Mahan, K., Newton, A.C., and Sassone-Corsi, P. (2010). Protein phosphatase PHLPP1 controls the light-induced resetting of the circadian clock. Proc. Natl. Acad. Sci. USA *107*, 1642–1647.

Miyoshi, Y., Yoshioka, Y., Suzuki, K., Miyazaki, T., Koura, M., Saigoh, K., Kajimura, N., Monobe, Y., Kusunoki, S., Matsuda, J., et al. (2014). A new mouse allele of glutamate receptor delta 2 with cerebellar atrophy and progressive ataxia. PLoS ONE *9*, e107867.

Monti, B., and Contestabile, A. (2000). Blockade of the NMDA receptor increases developmental apoptotic elimination of granule neurons and activates caspases in the rat cerebellum. Eur. J. Neurosci. *12*, 3117–3123.

Monti, B., Marri, L., and Contestabile, A. (2002). NMDA receptor-dependent CREB activation in survival of cerebellar granule cells during in vivo and in vitro development. Eur. J. Neurosci. *16*, 1490–1498.

Moran, J., and Patel, A.J. (1989). Stimulation of the N-methyl-D-aspartate receptor promotes the biochemical differentiation of cerebellar granule neurons and not astrocytes. Brain Res. *486*, 15–25.

Mulherkar, S.A., and Jana, N.R. (2010). Loss of dopaminergic neurons and resulting behavioural deficits in mouse model of Angelman syndrome. Neurobiol. Dis. *40*, 586–592.

Palkovits, M., Magyar, P., and Szentágothai, J. (1971). Quantitative histological analysis of the cerebellar cortex in the cat. II. Cell numbers and densities in the granular layer. Brain Res. *32*, 15–30.

Pennacchio, L.A., Bouley, D.M., Higgins, K.M., Scott, M.P., Noebels, J.L., and Myers, R.M. (1998). Progressive ataxia, myoclonic epilepsy and cerebellar apoptosis in cystatin B-deficient mice. Nat. Genet. *20*, 251–258.

Shimizu, K., Phan, T., Mansuy, I.M., and Storm, D.R. (2007). Proteolytic degradation of SCOP in the hippocampus contributes to activation of MAP kinase and memory. Cell *128*, 1219–1229.

Shmerling, D., Hegyi, I., Fischer, M., Blättler, T., Brandner, S., Götz, J., Rülicke, T., Flechsig, E., Cozzio, A., von Mering, C., et al. (1998). Expression of amino-terminally truncated PrP in the mouse leading to ataxia and specific cerebellar lesions. Cell *93*, 203–214.

Simonson, L., Baudry, M., Siman, R., and Lynch, G. (1985). Regional distribution of soluble calcium activated proteinase activity in neonatal and adult rat brain. Brain Res. *327*, 153–159.

Sobel, E., Sengul, H., and Weeks, D.E. (2001). Multipoint estimation of identity-by-descent probabilities at arbitrary positions among marker loci on general pedigrees. Hum. Hered. *52*, 121–131.

Song, M.S., Salmena, L., and Pandolfi, P.P. (2012). The functions and regulation of the PTEN tumour suppressor. Nat. Rev. Mol. Cell Biol. *13*, 283–296.

Stankewich, M.C., Gwynn, B., Ardito, T., Ji, L., Kim, J., Robledo, R.F., Lux, S.E., Peters, L.L., and Morrow, J.S. (2010). Targeted deletion of betaIII spectrin impairs synaptogenesis and generates ataxic and seizure phenotypes. Proc. Natl. Acad. Sci. USA *107*, 6022–6027.

Sun, J., Liu, Y., Moreno, S., Baudry, M., and Bi, X. (2015a). Imbalanced mechanistic target of rapamycin C1 and C2 activity in the cerebellum of Angelman syndrome mice impairs motor function. J. Neurosci. *35*, 4706–4718.

Sun, J., Zhu, G., Liu, Y., Standley, S., Ji, A., Tunuguntla, R., Wang, Y., Claus, C., Luo, Y., Baudry, M., and Bi, X. (2015b). UBE3A Regulates Synaptic Plasticity and Learning and Memory by Controlling SK2 Channel Endocytosis. Cell Rep. *12*, 449–461.

Wang, Y., Briz, V., Chishti, A., Bi, X., and Baudry, M. (2013). Distinct roles for μ-calpain and m-calpain in synaptic NMDAR-mediated neuroprotection and extrasynaptic NMDAR-mediated neurodegeneration. J. Neurosci. *33*, 18880–18892.

Wang, Y., Zhu, G., Briz, V., Hsu, Y.T., Bi, X., and Baudry, M. (2014). A molecular brake controls the magnitude of long-term potentiation. Nat. Commun. *5*, 3051.

Zhu, G., Liu, Y., Wang, Y., Bi, X., and Baudry, M. (2015). Different patterns of electrical activity lead to long-term potentiation by activating different intracellular pathways. J. Neurosci. *35*, 621–633.